1986

Deep Flow Variability in Central Drake Passage

John M. Klinck
Old Dominion University, jklinck@odu.edu

Eileen E. Hofmann
Old Dominion University, ehofmann@odu.edu

Original Publication Citation

Klinck, J.M., & Hofmann, E.E. (1986). Deep-flow variability at Drake Passage. *Journal of Physical Oceanography, 16*(7), 1281-1292. doi: 10.1175/1520-0485(1986)016<1281:DFVADP>2.0.CO;2

Deep-Flow Variability at Drake Passage

JOHN M. KLINCK AND EILEEN E. HOFMANN

Department of Oceanography, Texas A&M University, College Station, TX 77843

(Manuscript received 28 May 1985, in final form 31 January 1986)

ABSTRACT

A rotary empirical orthogonal function analysis of the currents measured in central Drake Passage during DRAKE 79 shows that the deep (2500 m) flow has the same spatial and temporal structure as the flow at 500 m, suggesting that current variability in this region penetrates to the bottom. However, comparison of the time amplitude of the corresponding modes indicates that the variability of the 2500 m flow resulting from north to south shifts in the location of the Polar Front lags that at 500 m by one to three days. This implies that the Polar Front slopes to the east or south (looking up from the bottom). A similar time structure was associated with the flow variations detected at moorings located downstream of a line of seamounts that extend into central Drake Passage. Additionally, the presence of mesoscale features (warm- and cold-core rings and meanders) can block or enhance the deep flow through the narrow channels separating the seamounts in Drake Passage. Such episodic changes in transport through channels has implications for deep water exchange between ocean basins, as determined from short-term current meter observations.

1. Introduction

As part of the final field experiment (DRAKE 79) of the International Southern Ocean Studies (ISOS) program, a large current meter array was deployed in Drake Passage (Fig. 1) for a period of one year, January 1979–February 1980. The purpose of the DRAKE 79 mooring array was to provide the spatial and temporal resolution necessary to monitor the transport of the Antarctic Circumpolar Current (ACC), meandering of the Polar Front and the mesoscale flow variability in the central passage region. To achieve these goals, the mooring array was composed of two parts. The Main Line (ML) moorings which extended across Drake Passage from Cape Horn to the South Shetland Islands were designed to monitor the transport of the ACC. The seven-mooring Mapping and Statistics (MS) array and the central portion of the ML array were located near the historical position of the Polar Front so as to monitor its variability as well as mesoscale activity in the central passage region. Horizontal mooring separations were based on previous estimates of the correlation length scales (Sciremammano et al., 1980) associated with temperature and flow fluctuations in Drake Passage. The central passage moorings were equipped with current meters at 500, 1400 and 2500 m; the remaining moorings had current meters at 500 and 2500 m.

The current and hydrographic data collected during DRAKE 79 and previous ISOS field studies have provided the basis for several investigations of the current variability in Drake Passage. From current measurements obtained in 1975, Bryden and Pillsbury (1977) considered the variability of deep (deeper than 2500 m) currents and showed that the rms variations associated with these currents are nearly equal to the yearlong mean. Moreover, their analysis indicated that these fluctuations occurred with a time scale of 15 days. Bryden (1979) further analyzed the deep currents in Drake Passage in terms of poleward heat flux and conversion of available potential energy by baroclinic instability. This analysis gave a time scale for growth of baroclinic instability of 15 days. However, a vertical phase difference in velocity variations, which is the signature of baroclinic instability, was difficult to observe in these data.

Wright (1981) considered a model of baroclinic instability for Drake Passage which included the simplifying assumption of no bottom topography. The results obtained from this model indicated that the flow in this region is baroclinically unstable. Comparison of the theoretical calculations with data obtained from a closely spaced cluster of current meters deployed in central Drake Passage during 1977 showed a good correspondence, probably because the 1977 array was located in a region of relatively flat topography. Wright also found that the energy removal rate calculated from the data decreased in the downstream (northeast) direction. Such a downstream decay occurs because the 1977 array was deployed east of a line of seamounts.

Inoue (1985) reconsidered the question of baroclinic instability in Drake Passage with the more extensive measurements obtained during DRAKE 79. On the basis of dynamical modal decomposition, he concluded that the flow is represented mainly by the barotropic and first baroclinic modes with the largest currents

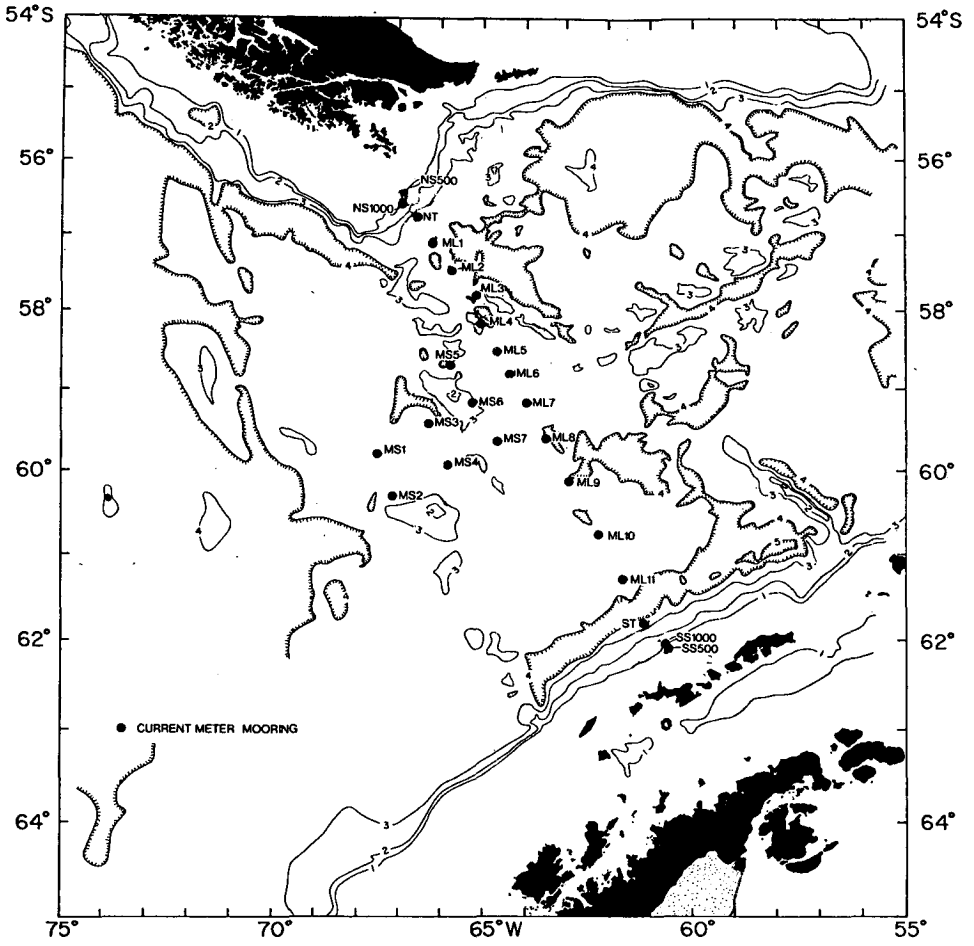

FIG. 1. Drake Passage and the location of DRAKE 79 current moorings.

being near the surface. His study of stability shows that the density distribution in the vicinity of the Polar Front is such that baroclinic instability is likely to occur with a growth rate of 14.6 days. Furthermore, two-thirds of the energy of the instability should be in the barotropic mode.

Hofmann and Whitworth (1985) described the current variations in central Drake Passage using weekly-averaged maps of water mass zonation which were constructed from temperature and velocity data obtained from the DRAKE 79 moorings. This analysis showed that variability in the central passage has two basic forms: that associated with north–south shifts of the Polar Front and that associated with the passage of warm- and cold-core rings and meanders. Furthermore, the trajectories followed by the rings are controlled by the rugged bottom topography within Drake Passage.

Klinck (1985) quantified the space and time structure of the flow in the central passage with an empirical orthogonal function (EOF) analysis. This study showed that migrations of the Polar Front occur approximately every three months and rings and meanders traverse the central passage region at regular intervals of one and a half to two months.

Rattray (1985), using the DRAKE 79 observations, analyzed the deep currents over the whole passage. This analysis indicated that the mean current associated with the deep flow tends to be along contours of constant f/depth. Furthermore, strong currents tend to occur in gaps between seamounts.

The results presented in this paper are a continuation of the investigation of flow in central Drake Passage begun by Klinck (1985), but with emphasis on the deep, 2500 m flow. Specifically, we are interested in the coupling between the 500 and 2500 m flow. There was an indication in the previous analysis that the upper and lower currents were decoupled. This result is at odds with Inoue's study which showed the flow at central passage moorings to be predominantly barotropic. A comparison of EOF structures and time series for the upper and lower current observations shows that there is a strong coupling but with a time shift. It is this time shift that gives the appearance in the full EOF analysis

that the two flows are decoupled. Also considered in this analysis is the response of 2500 m flow to the passage of mesoscale meanders and eddies and to the presence of bottom topography.

Section 2 describes the EOF analysis and the DRAKE 79 dataset. The results of the EOF and lagged correlation analyses are given in section 3. Section 4 presents a discussion of the results in terms of coupling between layers, steering by topography and influence of mesoscale features on deep flow. Section 5 is a summary.

2. Methods

a. Empirical orthogonal function analysis

Empirical orthogonal function analysis is a technique for reducing a large set of observations to a smaller set of patterns. Various studies that have used EOF analysis are discussed in Priesendorfer et al. (1981). In the present context, the EOF technique was used to convert a set of velocity time series at several locations into a set of spatial patterns of currents that have some temporal behavior. The analysis is sensitive to variance in the data and therefore, picks up the most energetic current patterns in the observations.

In contrast to Rattray (1985) who considered spatial patterns in the frequency domain, the EOF technique used here considers spatial patterns in the time domain. The EOF analysis employed by Rattray (1985) uses a Fourier transform of the current time series, while the EOF analysis used in this study is applied to the time series directly. In theory, the two techniques should be equivalent. However, the DRAKE 79 current observations are nonstationary in the statistical sense; the pattern of currents within Drake Passage changes three times during the experiment period because of north–south shifts in the location of the Polar Front (Hofmann and Whitworth, 1985; Rattray, 1985; Klinck, 1985). This low frequency (relative to the time series length) signal distorts the Fourier transform thereby making the spectra red. Indeed, Rattray notes "a general lack of coherence of the currents between stations with no clear robust patterns. . . ." As other analyses have found strong coherences in the Drake Passage data, the apparent lack of coherence in the DRAKE 79 data noted by Rattray (1985) is likely the result of the nonstationarity of the current observations. To avoid this problem, the present analysis proceeds in the time domain and uses lagged correlation analysis in place of coherence to detect correspondences between time series.

The application of EOF techniques to a two-dimensional vector time series is a direct extension of scalar EOF analysis (e.g., Legler, 1983). In general, this procedure considers velocity observations from a specific current meter as a time series of complex numbers. A data matrix is then constructed with each row composed of the complex time series from a given current meter. A complex, zero-lag, cross-correlation matrix is obtained by multiplying the data matrix by its complex conjugate transpose and dividing by the length of the time series.

The EOF modes which describe the dataset are the eigenfunctions of the cross-correlation matrix and the time variation of these modes is obtained by projecting the original data onto the eigenfunctions. The associated eigenvalues indicate the percentage of the total variance explained by a given eigenfunction, with the important modes associated with the larger eigenvalues. Because an EOF analysis generally yields several EOF modes, various selection rules provide a basis for determining which of the EOF modes are meaningful (Priesendorfer et al., 1981). In this study, the significant modes are determined from Monte Carlo calculations (Fig. 2) on random normal data matrices.

b. Current meter data

The actual sensor depth and the data record length for the meters comprising the 500 and 2500 m analyses are given in Table 1. The 40-hour low-pass filtered, daily-averaged velocity observations from these current meters were used for the EOF analysis. A complete discussion of the current meter data reduction and processing techniques is given in Pillsbury et al. (1981a,b) and descriptions of the DRAKE 79 array are given in Whitworth (1983) and Hofmann and Whitworth (1985).

As is apparent from Table 1, several data gaps exist in the velocity time series obtained from the 500 m sensors and one sensor from 2500 m, ML5, returned a shortened record. However, these gaps do not cause problems in the EOF analysis because the cross-correlation matrix is constructed by summing all possible products of observations at a given time. If no data exist for some time at a sensor, then there are simply fewer terms to sum to obtain the cross-correlation with the other time series. Therefore, EOF modes and amplitudes can be constructed for all sensors at each level for the duration of the longest time series, which in this analysis is 355 days.

3. Results of EOF and lagged correlation analysis

The EOF modes and time amplitudes are calculated for the 500 and 2500 m currents, separately. The record length mean has been removed from each time series. Therefore, the EOF modes represent variations from the mean and the structure of the currents represented by each mode is obtained by adding the mode currents (times an appropriate amplitude) to the mean.

The following sections describe the mean current pattern, the EOF modes and time behavior for each level and the correlations between the patterns observed in the two levels.

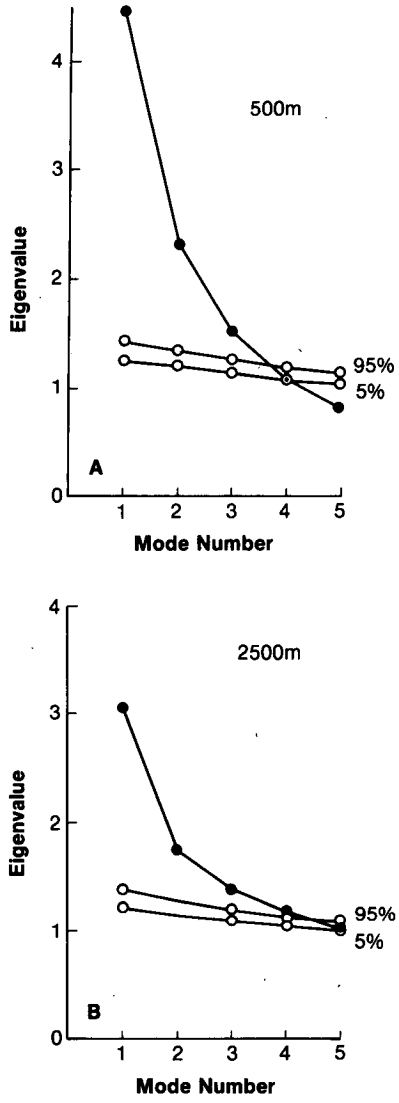

FIG. 2. Eigenvalues, normalized by mean variance, for the 500 and 2500 m EOF analysis. Open circles indicate the 5th and 95th percentile eigenvalues from a Monte Carlo calculation (100 trials, with unit normal random observations). (a) 500 m analysis using 13 sensors. The first three eigenvalues are significant. (b) 2500 m analysis using 11 sensors. The first four eigenvalues are significant.

a. Mean current structure

In general, the record length mean current for each meter at 2500 m (Fig. 3) is primarily through-passage (62°T). Exceptions are the flow at mooring MS5 which is directed across-passage to the southeast, the flow at mooring ML9 which exhibits a mean flow towards the west and flow at the upstream moorings, MS1 and MS2, which is directed northward. Each of these exceptions is the result of the steering of deep flow by bottom topography. Mooring MS5 was located in a channel between two seamounts which direct the flow southeastward and ML9 was located upstream of a large ridge which produces across-passage and westward flow (Reid and Nowlin, 1971; Rattray, 1985). Moorings MS1 and MS2 were located near a large seamount which causes a northward deflection of the flow in this region (Hofmann and Whitworth, 1985).

b. EOF modes of 2500 m currents

According to the Monte Carlo calculations (Fig. 2b), four of the EOF modes obtained from the 2500 m analysis are significant. The current meters which are represented by the individual modes can be determined by considering the amount of variance reduction produced by subtracting the EOF mode currents from the original velocity time series (Table 2). The significant modes primarily represent current variations from six sensors: ML5, ML6, ML7, ML9, MS5 and MS6. Thus, the velocity time series from these sensors account for most of the flow variability at 2500 m and each EOF mode represents principally currents from a single location or from two widely separated locations.

The first EOF mode explains 28% of the total variance of the entire dataset and represents the currents from MS5, which has the largest variance of the deep current records. The spatial pattern for this mode (Fig. 4a) indicates the dominance of the current at MS5 and the variance values given in Table 2 confirm that mode 1 represents the currents at MS5. Associated with this mode are strong directional changes (Fig. 5a) which occur over periods of five to ten days. The most pronounced of these are centered near days 40, 80, 155, 220, 275 and 330. Therefore, mode 1 represents one of two states; it either adds to or subtracts from the mean current. Because MS5 was located in a channel between two seamounts (cf. Fig. 3), a steady current might be expected at this location. However, the direction and amplitude time series indicate an episodic nature of the flow at MS5. In fact there is at times, a significant reduction of the flow and occasionally flow opposite to the mean current direction occurs.

The EOF mode 2 explains 16% of the total variance and represents flow variability primarily at ML5 but information from ML6 and MS6 (Table 2) is also included in this mode. The current pattern for mode 2 (Fig. 4b) indicates that all three of the represented currents flow basically in the same direction, with the magnitude of the flow variation decreasing to the south. Furthermore, the flow at these three moorings has basically the same time structure (Fig. 5b). The direction time series for this mode (Fig. 5b) indicates that over most of the 355 days, flow variability adds to the direction of the mean current. An exception to this occurs between days 80 and 150 when the flow direction is opposite to the mean current. This reversal is related to the Polar Front which was located south of ML5 between days 80 and 150 (Hofmann and Whitworth, 1985).

The third EOF mode accounts for 12% of the total dataset variance and represents principally flow vari-

TABLE 1. Sensor details at 500 and 2500 m.

	Mooring											
	ML5	ML6	ML7	ML8	ML9	ML10	MS1	MS2	MS3	MS4	MS5	MS6	MS7
500 m analysis													
Sensor depth (m)	644	685	575	607	608	498	685	800	645	500	752	814	540
Record length (year days)	34–388	34–388	34–361	34–333	34–388	34–388	34–185	34–385	34–387	34–156 225–333 367–385	34–388	34–388	34–385
2500 m analysis													
Sensor depth (m)	2644	2669	2593	No data	2665	2576	2685	2785	No data	2560	2752	2709	No data
Record length (year days)	31–358	31–385	31–385	—	31–385	31–385	31–385	31–385	—	31–385	31–385	31–385	—

ability at ML9 (Table 2), which was located in the southern end of the central passage. This mode also has some contribution from ML5 and ML7. The spatial pattern (Fig. 4c) indicates that current variations at ML9 tend to be opposite in direction from those at ML5 and at right angles to flow at ML7. Furthermore, the flow at ML9 is directed either northwest or south (Fig. 5c).

The last significant EOF mode explains 11% of the total variance and represents both ML6 and ML9 (Table 2). The spatial pattern (Fig. 4d) shows that current variations on the northern and southern sides of the central passage are in opposite directions.

The time series from modes 3 and 4 tend to be in quadrature, indicating that these two modes are parts of a traveling current pattern—two standing waves can add to form a single, moving current pattern. The interdependence of these modes is not quantified because the EOF time series are rather noisy, making the results of questionable value.

c. *Lagged correlations of 2500 m currents*

Temporal correspondences in flow activity among the various meters was determined from a lagged, rotary cross-correlation analysis of the time amplitudes of the 2500 m EOF modes. The significant peaks, as determined by the criterion of Sciremammano (1979), are listed in Table 3, excluding the zero lag inner correlations which will always be near unity. Inner (outer) correlations indicate that the time series rotate in the same (opposite) directions and positive lags occur when the first series leads the second.

On the basis of the significant time lags, correlations can be grouped into three categories: less than 2 weeks, 2 weeks to 2 months and longer than 3 months. Each of these time scales is associated with a different character of the current variability.

There are three instances of significant outer autocorrelations with lags of zero to two days. The outer correlation of mode one with itself at zero lag means that the currents represented by this mode tend to be in one of two directions along a line (rectilinear currents). This result is not surprising since mode 1 represents primarily the flow at MS5 which is strongly affected by the channel in which the mooring was placed. Two other outer autocorrelations occur (modes 2 and 4) with a 2-day lag. Such a relationship could indicate a tendency for the flow to be bi-directional, but the more likely explanation is that this reflects the time required for the flow at these locations to change direction, as when the Polar Front shifts. The remaining significant peaks for lags shorter than two weeks indicate primarily travel time of variability between moorings.

The only two short time cross-correlations occur between mode 3 (ML9) and mode 4 (ML6). The 3-day (inner) peak represents the travel time associated with

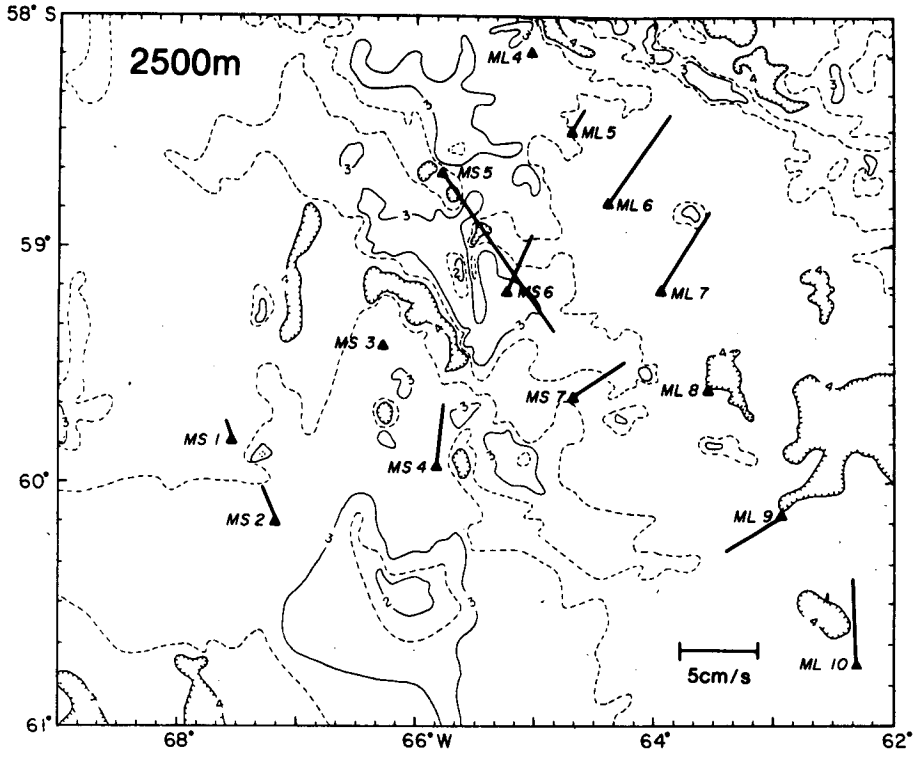

FIG. 3. The mean velocity vectors obtained from the 11 current meter records from 2500 m. Depth contours are given in 500 m (dashed) and 1000 m (solid) intervals.

migrations of the Polar Front between these two moorings. The 11-day outer correlation between these modes is associated with the time delay for mesoscale current variations between the two moorings. Since ML7 is not strongly represented by an independent EOF mode, it is not possible to apply a consistency argument to this result. Furthermore, it is likely that the DRAKE 79 current observations do not have the spatial coverage necessary to resolve the transient current pattern associated with Polar Front movement between ML5 and ML9.

TABLE 2. Variance analysis for the significant EOF modes from 2500 m.

Mooring	Total variance	Residual after fitting EOF modes 1	2	3	4	Variance explained (%)	Modes
ML5	27.5	30.8	11.2	6.6	4.3	85	2, 3
ML6	20.6	20.2	15.7	16.5	11.8	42	2, 4
ML7	20.1	18.7	20.1	14.4	13.4	33	3
ML9	23.0	22.2	20.6	9.1	3.1	87	3, 4
ML10	17.2	16.2	15.5	15.5	14.5	16	
MS1	8.8	9.0	9.0	9.0	8.6	2	
MS2	7.0	7.4	6.9	6.8	6.6	6	
MS4	12.5	12.6	12.3	11.5	10.5	16	
MS5	50.2	7.3	3.7	3.3	2.6	95	1
MS6	14.4	13.4	11.4	11.5	11.0	24	2
MS7	9.8	10.8	12.0	13.0	13.0	—	

The significant intermediate (2 weeks to 2 months) time lags fall into two categories; flow variability on time scales of 20–30 days and 50–60 days. All of these correlations, with one exception, are outer correlations which correspond to current changes with opposite rotations. The single exception, 1 versus 3 inner and outer, occurs because mode 1 is correlated with itself at zero lag and, therefore, should have both inner and outer correlations with any other mode. These intermediate lag correlations show that the effects of the warm- and cold-core rings, which occur approximately every 60 days in the central passage, penetrate to the bottom.

The long time lag correlations (greater than 3 months) occur at 100 and 200 days and represent the time between shifts of the Polar Front from ML5 to ML7. The 200-day (inner) correlation is a harmonic which represents the time between two frontal shifts in the same direction. The long-time correlation peaks do not occur exactly at the same lag because of varying propagation times between moorings.

d. EOF modes of 500 m currents

The EOF modes for 500 m currents correspond quite closely to the modes of the full analysis presented in Klinck (1985). The reason for this correspondence is that an EOF analysis fits the largest variance in the data which, in this case, occurs in the 500 m obser-

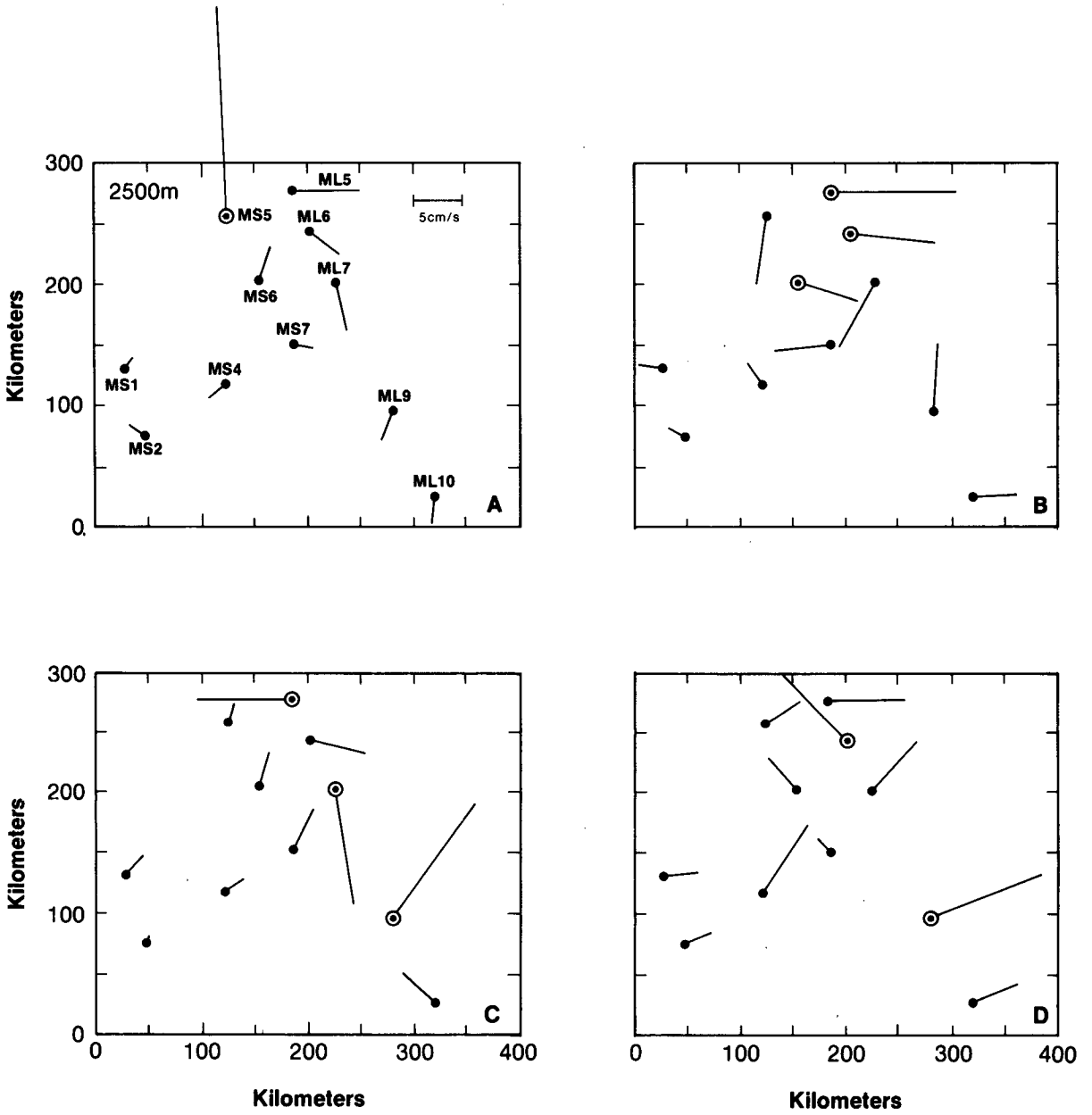

FIG. 4. EOF current structure for the four significant modes for the 2500 m analysis. The absolute length of the vectors is arbitrary, but the relative length and direction are meaningful. The open circles indicate the mooring locations at which an EOF mode explains more than 20% of the residual variance. (a) EOF mode 1, (b) EOF mode 2, (c) EOF mode 3, (d) EOF mode 4.

vations. Therefore, the 500 m current variance dominates the full analysis; hence, the close correspondence. This analysis is different in that only the first three modes are significant (Fig. 2a), in contrast to 5 in the full analysis. The difference results from the smaller number of sensors used for the 500 m analysis (13) compared to the full analysis (33).

The first mode explains 28% of the total dataset variance and represents the Polar Front when it is near ML5 and ML6. The time structure of this mode is approximately the same as mode 1 of the full analysis. The EOF mode 2 explains 16% of the total variance in the 500 m analysis and represents mainly the Polar Front near ML7. The time structure of mode 2 is similar to that of mode 1 except that the direction series has the opposite sign. Therefore, modes 1 and 2 of the 500 m analysis represent the northern and southern positions of the strong current associated with the Polar Front. Mode 3 accounts for 13% of the total variance and the time structure of this mode reveals that it rep-

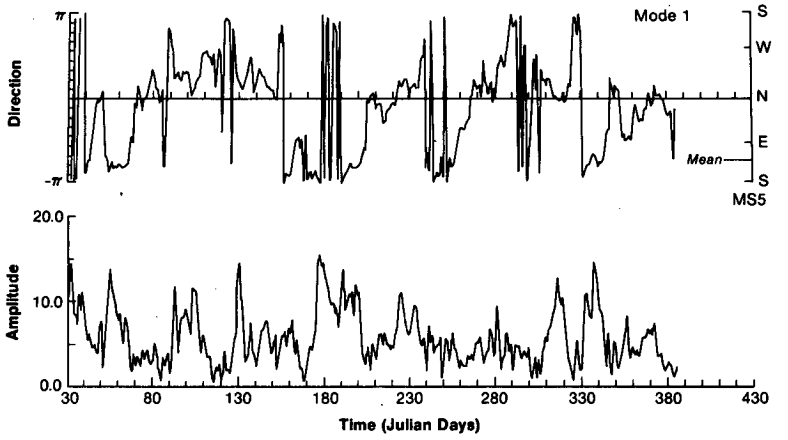
Mode 1
Direction
π
-π
S
W
N
E
S
Mean
MS5
Amplitude
20.0
10.0
0.0
30
80
130
180
230
280
330
380
430
Time (Julian Days)

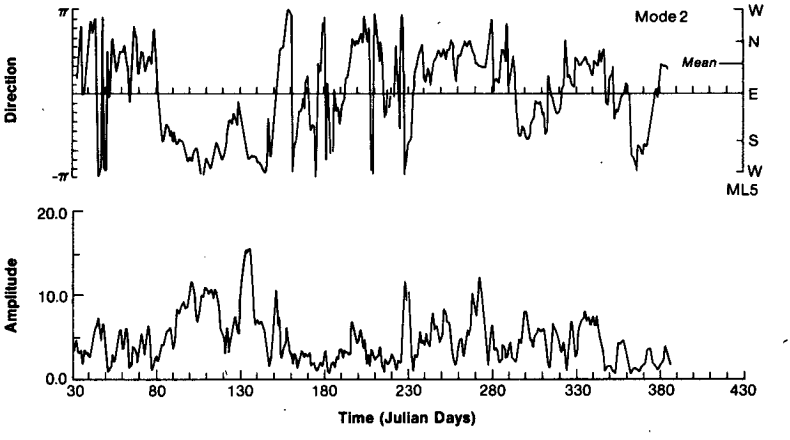
Mode 2
Direction
π
-π
W
N
Mean
E
S
W
ML5
Amplitude
20.0
10.0
0.0
30
80
130
180
230
280
330
380
430
Time (Julian Days)

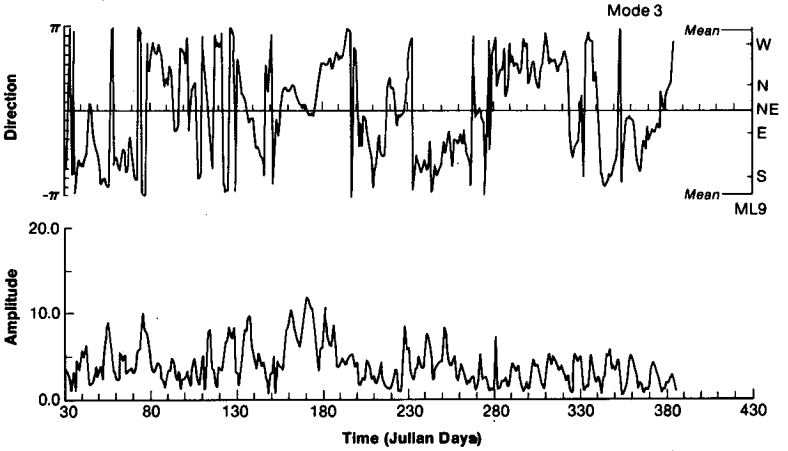
Mode 3
Direction
π
-π
Mean
W
N
NE
E
S
Mean
ML9
Amplitude
20.0
10.0
0.0
30
80
130
180
230
280
330
380
430
Time (Julian Days)

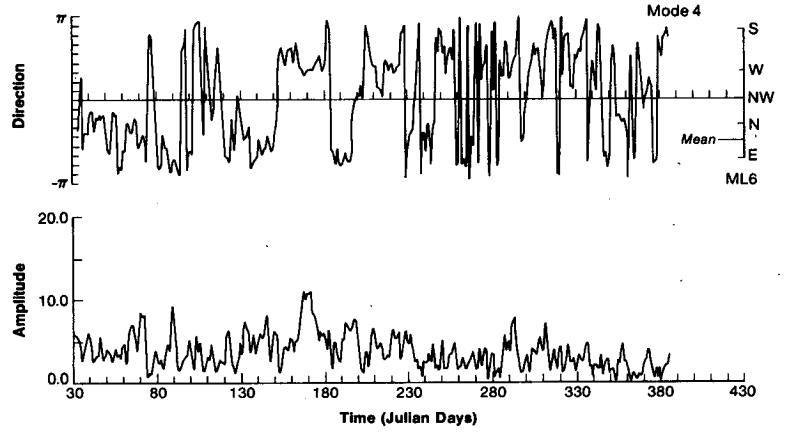
Mode 4
Direction
π
-π
S
W
NW
N
Mean
E
ML6
Amplitude
20.0
10.0
0.0
30
80
130
180
230
280
330
380
430
Time (Julian Days)

TABLE 3. Cross correlations for 2500 m EOF modes.

Mode	Lag (day)	Type
1 vs 1	0	outer
2 vs 2	+2	outer
3 vs 3	+105	outer
4 vs 4	+2	outer
1 vs 3	+21	inner
1 vs 3	+21	outer
1 vs 3	−124	outer
1 vs 4	+58	outer
2 vs 4	+201	inner
2 vs 4	+34	outer
2 vs 4	−65	outer
3 vs 4	+3	inner
3 vs 4	+11	outer
3 vs 4	+41	outer
3 vs 4	−92	outer

TABLE 4. Cross correlations for 500 m EOF modes.

Mode	Lag (day)	Type
2 vs 2	0	outer
1 vs 2	−2	inner
1 vs 3	+129	outer
2 vs 3	+144	outer

resents the current variability due to rings and meanders in the vicinity of ML5, ML6, ML7 and MS5. This mode corresponds closely to mode 2 of the full analysis.

e. *Lagged correlations of 500 m currents*

The lagged correlation analysis for the three significant modes at 500 m are shown in Table 4. There are fewer peaks in the correlations because of the smaller number of significant modes. The peaks indicate only short and long time scales, with no intermediate scale peaks. Recall that only one mode (mode 3) represents mesoscale variability so there are fewer opportunities for significant correlations than at 2500 m where four of the modes contained intermediate time scale variations. Therefore, the correlations of the 500 m EOF modes reflect primarily the variability associated with shifts of the Polar Front.

The short time lags indicate rectilinear change at ML7 (mode 2) and a travel time between ML5 and ML7 associated with the disturbances resulting from the Polar Front shift. The negative lag for the correlation between modes 1 and 2 indicates that the disturbance occurs first at ML7.

The long lags represent a combination of scales associated with the movement of the Polar Front and the passage of rings. Mesoscale current variations have a different character depending on the location of the Polar Front which, as noted by Klinck (1985) and Rattray (1985), tends to be in one of two gaps in the topography of the central passage. The two long time lags represent the time between front shifts plus half of the average time between rings.

f. *Lagged correlations of 500 versus 2500 m currents*

The time behavior of each of the EOF analyses for the two levels is similar. Flow variability occurs in one of three time bands which represent travel time between mooring locations and the time scales associated with successive rings and frontal shifts. Since the same kind of variability is observed at 500 and 2500 m, there should be some correlations between the EOF analyses for each depth. Significant lagged correlations between these two levels are given in Table 5. As with the other analyses, the significant peaks separate into three time bands: less than 1 week, 1 to 2 months and longer than 3 months.

The short time lags indicate travel time between meters. Those modes that represent variability at the two levels for the same mooring show how flow features propagate past the mooring. For example, the 2-day (inner) correlation between 1–5 (ML5) and 2–25 (ML5) shows that the frontal shift occurs first near the surface. This time lag is interpreted as being due to a tilting or slope of the front. A similar time lead for mesoscale variations at 500 m is shown by the outer correlation of 3–5 (ML5) and 4–25 (ML6).

The intermediate time scale peaks occur because of mean time between rings (about 60 days) plus time delays for travel. The 30-day correlations arise from correlations of opposite sides of a given ring or from the trailing edge of one ring with the leading edge of the following ring.

Long time scale lags represent variability associated with north-south shifts of the Polar Front. The time scale between shifts is about 100 days. The lags in this analysis range over 100 to 140 days. This smearing of the front shift signal results from aliasing by vertical lags associated with mesoscale variability.

FIG. 5. Direction and amplitude for the time variation of each of the four significant EOF modes from the 2500 m analysis. The units of the amplitude series are arbitrary. The direction series are rotations relative to the spatial structure shown in Fig. 4. An absolute direction scale for the sensor that has the most variance explained by the mode is included on the right. The time axis is in Julian days with day 1 corresponding to 1 January 1979. (a) EOF mode 1, (b) EOF mode 2, (c) EOF mode 3, (d) EOF mode 4.

TABLE 5. Cross correlations of the 500 and 2500 m time series obtained from the EOF analyses.

Mode	Lag (days)	Type
1_5 vs 2_{25}	+2	inner
1_5 vs 4_{25}	+39	outer
2_5 vs 1_{25}	+136	outer
2_5 vs 2_{25}	−2	inner
2_5 vs 3_{25}	−3	inner
2_5 vs 3_{25}	+114	outer
2_5 vs 4_{25}	+67	outer
3_5 vs 1_{25}	−62	outer
3_5 vs 1_{25}	−145	outer
3_5 vs 2_{25}	+21	outer
3_5 vs 3_{25}	−28	outer
3_5 vs 3_{25}	−43	outer
3_5 vs 3_{25}	−88	outer
3_5 vs 3_{25}	−104	outer
3_5 vs 3_{25}	−112	outer
3_5 vs 3_{25}	−120	outer
3_5 vs 3_{25}	−132	outer
3_5 vs 4_{25}	+3	outer

4. Discussion of results

a. Coupling of 500–2500 m flow

In the EOF analysis of the full central passage data set, there was very little apparent coupling between the 500 and 2500 m currents. Yet independent analyses of currents at these levels are similar. Lagged cross correlations of the independent EOF modes indicate that the flow is indeed related but shifted slightly in time (Table 5). This temporal shift is sufficient to prevent similar flow variability at the two levels from appearing in the same mode, since EOF structure is based on the zero-lag correlation matrix. The currents at the two levels, thus, appeared to be decoupled.

Two kinds of flow variations are indicated by the EOF analysis: shifts of the Polar Front and passage of rings and meanders. Both of these variations show vertical correlations with time lags of a few days. Furthermore, the timing is such that the changes occur near the surface first. This time lag is interpreted as a slope in the Polar Front and its associated current, with the front sloping south and east (looking up from the bottom). This is a hydrostatically consistent situation with warm (northern) water overlying cold (southern) water. During a southward shift of the front (of which there are two in the record), current changes appear first at the upper level. There is also an indication of southeastward lean in the mesoscale features [for example, 3–5 (ML5) versus 4–25 (ML6)]. As these rings and meanders move through-passage to the northeast, the disturbance appears at 500 m a few days before it appears at 2500 m. This is counter to the expectation that the disturbance due to a baroclinic instability leans against the flow which in this case would yield a westward lean (Bryden, 1979; Wright, 1981).

The resolution of this problem is that these mesoscale features are proposed to be the near field of topographic lee waves produced by the series of seamounts running through the central passage. McCartney (1975) analyzed topographic lee waves with a two-layer numerical model for the Northern Hemisphere. His simulations (see his Fig. 7) correspond reasonably well with conditions in Drake Passage, though his solutions must be reflected through a horizontal line to correspond to the Southern Hemisphere. His model parameter b gives the square of the ratio of the width of the bump to the lee wave scale $(u_0/\beta)^{1/2}$, where u_0 is the speed of the incoming flow and β is the gradient of the Coriolis parameter. For a 50 km wide seamount, typical of the seamounts in the central passage, the leewave scale for his simulations ($b = 0.31$) is approximately 90 km.

The Rossby wake described by McCartney (1975) is vertically coherent. The vertical lag obtained from the cross correlation analysis of the DRAKE 79 data indicates that the Rossby wake is offset in the vertical. Advective effects could push the wake downstream thereby producing an offset. The "pushing" of the Taylor columns off of topography by advective processes was observed in the one-layer numerical model presented by Huppert and Bryan (1976). In a similar manner, the Rossby wakes can be affected by the vertical shear such that the upper layer wake is pushed downstream relative to the lower layer, producing the observed lean. Such an advective effect in Taylor columns is discussed by Lighthill (1970).

Wright (1981) analyzed current data from the closely spaced current meter array deployed in Drake Passage in 1977. The array was centered at 59°06′S, 63°49′W which places it north and east of ML7 in a relatively flat region of the central passage. Wright's analysis concluded that the flow variability in this region was due to baroclinic instability. The lee wave hypothesis presented above is consistent with a baroclinic instability mechanism. The flow in central Drake Passage is baroclinically unstable as has been found by numerous investigators. However, the seamounts act as a tripping mechanism for the flow, producing perturbations with length scales of 50–100 km which match the length scales of most unstable baroclinic instability. The observations in the central passage at the DRAKE 79 moorings, ML5–ML6, represent the near field of the topographic wake; the observations from 1977 are downstream sufficiently for the instability mechanism to dominate.

There is support in the hydrographic data for a shifted lee wave in this region. The dynamic height fields for 2500 m relative to 3000 m and 3500 m relative to 3000 m (Fig. 6; Whitworth, personal communication, 1985) from data taken in January and February 1977 indicate a wavy downstream structure. Furthermore, the two fields are shifted by about one half of a wave length.

b. Effect of mesoscale features

The EOF mode 1 from the 2500 m analysis, which primarily represents MS5, reveals a strong current

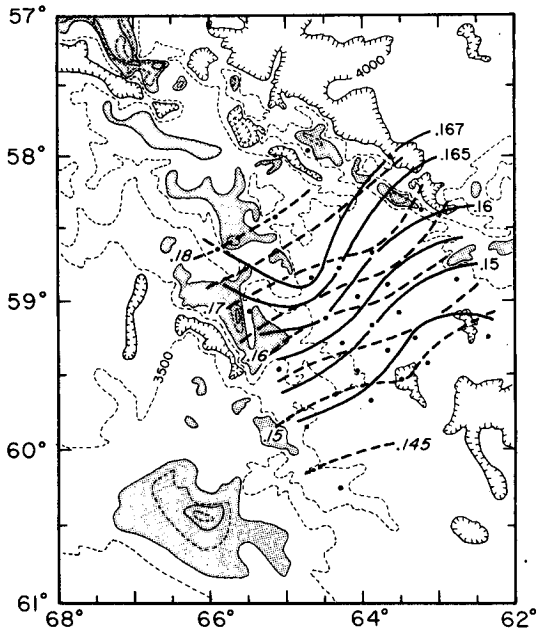

FIG. 6. Dynamic height field calculated from a grid of hydrographic stations occupied in central Drake Passage, January and February 1977. Dashed contours show the dynamic topography of 2500 m relative to 3000 m and solid contours show 3000 m relative to 3500 m.

variability that either opposes or enhances the mean current (Fig. 5a). For a large enough modal amplitude, the current can be upchannel (northwestward) opposite to the mean current. Mooring MS5 was located on the northern edge of the MS array along the trajectory preferred by warm- and cold-core rings and meanders as they traversed Drake Passage (Hofmann and Whitworth, 1985). The pressure gradient associated with these features seems to enhance or retard the flow at MS5 depending on the location of the feature relative to the mooring. The presence of a cold-core feature to the north or east of MS5 will decrease the flow; whereas, a warm-core feature at the same location will increase the flow. Similarly, a cold (warm) feature to the south or west will increase (decrease) the flow.

The effect of mesoscale features on the flow at MS5 is seen in the 2500 m current records that have been rotated such that the velocity components are aligned downchannel (Fig. 7). The times when mesoscale features were present at MS5 are indicated. The following discussion will focus on the first part of the current meter record. Patterns depicted here are representative of those in the latter portion.

During February 1979, a deep, warm meander—the core of which was east of MS5—dominated the circulation in the central passage (Hofmann and Whitworth, 1985). The result was increased downchannel flow at MS5. Once the warm meander departed Drake Passage (early March) the downchannel velocity at MS5 decreased to approximately 10 cm s^{-1}, which is approximately the record-length mean velocity. Following the warm meander was a warm-core ring which was, in turn, followed by a cold-core ring. The warm-core ring passed to the south of MS5 and the cold-core ring passed to the north of MS5. These two features essentially blocked the flow down the channel and produced a slight upchannel flow. Similar arguments can be made for the remaining periods when mesoscale features were present at MS5. The increased downchannel flow in mid-July and November also coincides with times when the Polar Front, having migrated northward, was located near MS5. The presence of this intense current substantially increased flow through the channel.

5. Summary

The vertical coherence of individual mesoscale features in Drake Passage has been noted by Peterson et al., (1982) and Bryden (1983) indicates that such coherence may be typical of features in the ACC. The EOF analysis of the DRAKE 79 current observations quantifies the strong vertical coupling of the flow in central Drake Passage. However, there are time lags associated with the flow variations which, if not taken

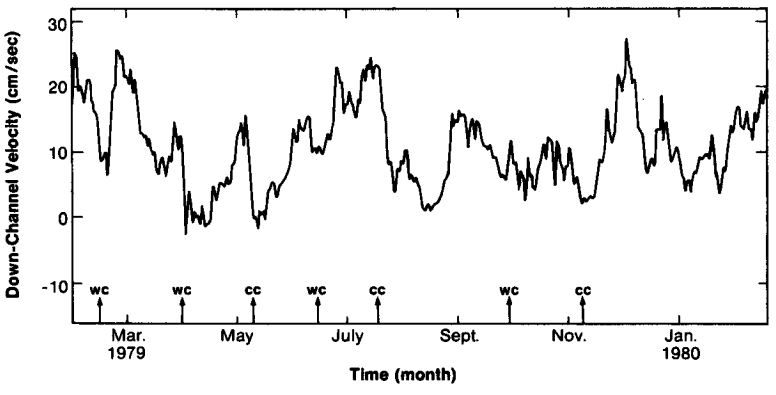

FIG. 7. Time series of downchannel flow at 2500 m from mooring MS5. Arrows indicate times when warm-core (wc) and cold-core (cc) features were present at this mooring. See Hofmann and Whitworth (1985) for a discussion.

into account, produce an apparent decoupling between the upper and lower layer.

The strongest flow variations (largest variance) occurred at moorings ML5, ML6, ML7 and ML9 which were located downstream of a line of seamounts that extend through central Drake Passage (Fig. 1). Furthermore, the lagged cross-correlation analysis of the time structure of the currents at these mooring locations indicates that flow variations in this region lean downstream (south or east). If this variability were the result of the baroclinic instabilities, then one would expect to detect an upstream lean (Pedlosky, 1979; Bryden, 1979). However, if the variability at the moorings is the result of topographically-forced lee waves, then a downstream tilt would be expected. Support for a lee wave hypothesis is provided by the dynamic topography (Fig. 6) in this region. By comparison, moorings MS1 and MS2, which were located at the western edge of the MS array in the vicinity of a large seamount, did not show a similar variability. This suggests that flow variations detected by the DRAKE 79 mooring array are triggered by the local bottom topography and are not advected into the passage.

The lagged cross-correlation analysis of the EOF modes associated with movement of the Polar Front indicates that the flow variations associated with this shift occur first at the upper layer. The implication is that the Polar Front is sloped either to the east or south. This slope is consistent with the observed vertical shear of geostrophic flow in this region (Whitworth, 1983).

A final conclusion from this study is that mesoscale features can block or enhance flow in narrow, deep channels. Such episodic changes in transport through channels has implications for deep water exchange between ocean basins as determined by short current meter records.

Acknowledgments. Support for this project was provided by National Science Foundation Grant OCE-8307959. We thank Tom Whitworth, III for providing Fig. 6.

REFERENCES

Bryden, H. L., 1979: Poleward heat flux and conversion of available potential energy in Drake Passage. *J. Mar. Res.*, **37**, 1–22.

——, 1983: The Southern Ocean. *Eddies in Marine Science*, A. R. Robinson, Ed., Springer-Verlag, 265–277.

——, and R. D. Pillsbury, 1977: Variability of deep flow in the Drake Passage from year-long current measurements. *J. Phys. Oceanogr.*, **7**, 803–810.

Hofmann, E. E., and T. Whitworth, III, 1985: A synoptic description of the flow at Drake Passage from year-long observations. *J. Geophys. Res.*, **90**, 7177–7188.

Huppert, H. E., and K. Bryan, 1976: Topographically generated eddies. *Deep-Sea Res.*, **23**, 655–679.

Inoue, M., 1985: Modal decomposition of the low-frequency currents and baroclinic instability at Drake Passage. *J. Phys. Oceanogr.*, **15**, 1157–1181.

Klinck, J. M., 1985: EOF analysis of central Drake Passage currents from DRAKE 79. *J. Phys. Oceanogr.*, **15**, 288–298.

Legler, D. M., 1983: Empirical orthogonal function analysis of wind vectors over the tropical Pacific region. *Bull. Amer. Meteor. Soc.*, **64**, 234–241.

Lighthill, M. J., 1970: The theory of trailing Taylor columns. *Proc. Cambridge Phil. Soc.*, **68**, 485–491.

McCartney, M. S., 1975: Inertial Taylor columns on a beta plane. *J. Fluid Mech.*, **68**, 71–95.

Pedlosky, J., 1979: *Geophysical Fluid Dynamics.* Springer-Verlag. 624 pp.

Peterson, R. G., W. D. Nowlin, Jr. and T. Whitworth, III, 1982: Generation and evolution of a cyclonic ring at Drake Passage in early 1979. *J. Phys. Oceanogr.*, **12**, 712–719.

Pillsbury, R. D., J. S. Bottero and R. E. Still, 1981a: Current, temperature and pressure in the Drake Passage during DRAKE 79, January 1979–January 1980, Volume XIV, Part A. Oregon State University Data Rep., No. 81-17, 374 pp.

——, —— and ——, 1981b: Current, temperature and pressure in the Drake Passage during DRAKE 79, Volume XIV, Part B. Oregon State University Data Rep., No. 81-17, 216 pp.

Priesendorfer, R. W., F. W. Zwiers and T. P. Barnett, 1981: Foundations of principal component selection rules. SIO Ref. Ser. 81-4, Scripps Institution of Oceanography, 192 pp.

Rattray, M. Jr., 1985: The effect of bathymetry on the deep flow in Drake Passage. *Deep-Sea Res.*, **32**, 127–147.

Reid, J. L., and W. D. Nowlin, Jr., 1971: Transport of water through the Drake Passage. *Deep-Sea Res.*, **18**, 51–64.

Sciremammano, F., Jr., 1979: A suggestion for the presentation of correlations and their significance levels. *J. Phys. Oceanogr.*, **9**, 1273–1276.

——, R. D. Pillsbury, W. D. Nowlin, Jr. and T. Whitworth, III, 1980: Spatial scales of temperature and flow in Drake Passage. *J. Geophys. Res.*, **85**, 4015–4028.

Whitworth, T., III, 1983: Monitoring the transport of the Antarctic Circumpolar Current at Drake Passage. *J. Phys. Oceanogr.*, **13**, 2045–2057.

Wright, D. G., 1981: Baroclinic instability in Drake Passage. *J. Phys. Oceanogr.*, **11**, 231–246.